STEADY STATE SIMULATION OF DESSULFURIZATION IN CIRCULATING FLUIDIZED BEDS

Christian Coelho da Costa Milioli
Group and Thermal and Fluids Engineering, School of Engineering of São Carlos, University of São Paulo, Av. Trabalhador São-carlense 400, 13566-590, São Carlos - SP, Brazil.
e-mail: ccosta@sc.usp.br

Fernando Eduardo Milioli
Group and Thermal and Fluids Engineering, School of Engineering of São Carlos, University of São Paulo, Av. Trabalhador São-carlense 400, 13566-590, São Carlos - SP, Brazil.
e-mail: milioli@sc.usp.br

Abstract. *Two-fluid modeling was applied through CFX 5.7 to simulate steady state dessulfurization in circulating fluidized bed risers at conditions typical of coal combustion. Various operational conditions were simulated, comprising different reactor diameters (7,62 and 76,2 cm) and heights (5.56 and 15 m), and different particulate sizes (210 and 520 μm). Steady state convergence was achieved in only one of the considered cases. An uniform flow was found which is not physically realistic for risers. The anomalous convergence was attributed to numerical diffusion. Contrary to the converged case, the non converged cases provided flows characterised by the development of coherent structers. The predictions indicate that whenever coherent structures are formed residence times grow up and sulfur removal is improved.*

Keywords*: two-fluid modeling, circulating fluidized bed, dessulfurization, steady state simulation, CFX.*

1. Introduction

The application of fluidized beds to gas-solid reactive processes requires the utilization of high charges of solids to provide high contact area between phases, intense mixture to maximize mass and energy transport, and residence time sufficient enough so that the chemical reactions can develop at the desired extent. Fluidized bed reactors can operate in different hydrodynamic regimes, characterized by different flow patterns. As the flow rate of the carrying gas is raised, the hydrodynamic pattern progressively goes through fixed, minimum fluidized, bubbling, turbulent and finally fast or circulating fluidized bed. Further increases in gas flow rate leads to pneumatic transport. Concerning heterogeneous reactive processes, the best fluid flow conditions simultaneously satisfying the requirements of charge, contact area and residence time, are found in circulating fluidized beds. In view of that, circulating fluidized beds are widely applied in processes such as petroleum catalytic cracking, coal combustion and gas cleaning.

The circulating fluidized beds may be classified as low density or high density. The high density beds are generally applied to processes involving gas-solid reactions, such as coal combustion and dessulfurization by limestone. The low density beds are generally applied to catalytic processes such as petroleum cracking. In the gas-solid reactive processes the relatively slow chemical kinetics requires higher residence times of the solids. As a consequence, lower gas velocities are applied (5 to 9 m/s) and/or coarser particulates are used (200 to 1000 μm). Otherwise, in catalytic processes, characterized by relatively quicker kinetics, lower residence times are required. As a consequence, higher gas velocities are applied (6 to 28 m/s) and/or finer particulates are used (40 to 100 μm). Considering the gas velocities and the particulate sizes applied, the solid circulation rates result typically between 10 and 100 kg/m^{2}s in low density beds, and between 400 and 1200 kg/m^{2}s in high density beds (Sun, 1996). The average concentration of solids in low density beds is typically below 3%, while in high density beds it can be as high as 20 % (Grace and Bi, 1997). The choice of the cross section of a reactor is mainly related to the required yield (e.g. the amount of gasoline and other derivatives in petroleum catalytic cracking, heat in coal combustion, SO_2 removal in dessulfurization), while the height of a reactor is mainly related to the required residence time.

In this work the concern is turned to the investigation of the effects of the hydrodynamics on the rate of reaction in gas-solid reactions. The application of interest is the absorption of SO_2 by limestone in conditions typical to fluidized bed coal combustion. Numerical simulation is carried out applying two-fluid modeling through CFX 5.7. Different scales of reactor and particulate sizes are considered, which considerably affect hydrodynamics and then chemical reaction rates in the reactor.

2. Two-fluid modeling with chemical reaction

Two-fluid models for gas-solid flows are developed from integral mass and momentum balances over suitable control volumes comprising all the phases (see, for instance, Enwald *et al*., 1996, Gidaspow, 1994). The theorems of Leibniz and Gauss are applied to the integral balances giving rise to local instantaneous conservative equations for each phase and jump conditions describing interface interactions among phases. Then, averaging procedures are applied

providing averaged equations. Closure laws are included to deal with parameters and coefficients required by the governing equations, and boundary and initial conditions are specified. The closure laws provide correlations and data for viscous stress tensors, viscosities, pressures and drag. Alongside with the continuum hypothesis, all the phases are commonly assumed Newtonian-Stokesian. Solid phases are generally assumed to be comprised of homogeneous uniform particles. In general, three different effects are considered for defining the pressure of the solid phase: momentum transfer owing to particle velocity fluctuations, particle to particle collisions, and gas phase pressure. The first effect is generally disregarded, and the particle to particle collision is modeled in terms of an elasticity modulus correlated from experiment. Pressure and viscosities of the solid phase are commonly taken from experiment. Otherwise, pressure and viscosities of the solid phase may also be determined through theoretical correlations as a function of a granular temperature, obtained through analogies between the granular flow and the flow of dense gases (Jenkins and Savage, 1983, Lun *et al.*, 1984). A stationary interface drag force, empirically correlated, accounts for the interface momentum transfer between the gas and the solid phases. Wall boundary conditions for the solid phase are commonly determined considering either free slip or partial slip conditions.

Mass balances for different chemical species inside each phase provide species continuity equations required in reactive simulations. Also, due to chemical reaction additional terms are included into the continuity and momentum equations for each phase. Table 1 shows the formulation which is used in this work.

2.1. Gas-solid two-fluid ractive modeling with CFX 5.7

CFX 5.7 incorporates hydrodynamic two-fluid model A as described in Tab. 1 (CFX 5.7, 2004a, 2004b). Besides multiphase, the models are also multi-species. Any number of different species may be considered inside any number of different phases. Mass transfer may be considered between species inside a phase and between species of different phases, so that both phase and interphase chemical reaction may be accounted for. Different turbulence models may be applied for any phase. Different interphase drag models may be applied, including Gidaspow´s model as included in Tab. 1. Besides the drag force, other intherphase forces may be accounted for such as lift, virtual mass, wall lubrication and turbulent dispersion forces (those are generally disregarded in gas-solid flows). Solid phase pressure may be accounted for through different procedures for determining the particle-particle elasticity modulus, including Gidaspow and Ettehadieh's model as given in Tab. 1. Conservative equations may be included to determine granular temperatures, so that correlations for solid phase pressure and viscosity based on granular temperature may be implemented. Only the features accounted for in Tab. 1 are considered in this work.

Element-based finite volume discretization is applied (CFX5.7, 2004c). Non-structured meshes are applied in Cartesian coordinate system. Tetrahedral, hexahedral, prismatic or pyramidal mesh elements may be used. The median method is applied to define control volumes over which the conservative equations are integrated to obtain the discretized equations. Interpolations of convective terms are performed through first order upwind or higher order schemes. Time interpolations may be performed through first or second order schemes. The discretized equations are solved implicitly through direct methods applying matrix inversion techniques. As a consequence, couplings such as pressure $\times$ velocity and drag are straightly solved, and iteration is only required to overcome non-linearities.

3. Test cases

The operating conditions described by Tsuo (1989) and Therdthianwong (1994) are considered. Tsuo performed two-fluid Eulerian hydrodynamic simulations of the gas-solid flow in a small scale circulating fluidized bed 7.62 cm diameter and 5.56 m high. Applied 520 μm mean size particulate and a solid's circulation rate of 24.9 kg/m^{2}s, which are conditions typical of circulating fluidized bed coal combustion. Therdthianwong carried out a two-fluid Eulerian simulation of SO_2 absorption by limestone in a circulating fluidized bed combustor of commercial dimensions, 3 m diameter and 15.5 m high. Applied 210 μm mean size particulate, which is adequate to circulating fluidized bed coal combustors. However, Therdthianwong applied a solid circulation rate of approximately 510 kg/m^{2}s, out of range by far compared to the usual for circulating fluidized bed coal combustion (10 to 100 kg/m^{2}s).

In Tsuo's simulations the reduced diameter of the reactor imposes excessive wall effect. The importance of such effect on hydrodynamics and reactive processes may be evaluated simulating different scales of reactor and comparing results. As a larger scale it would be interesting to simulate commercial scales, such as that considered by Therdthianwong. However, in Therdthianwong's scale a very coarse computational mesh is required, which is imposed by the huge dimensions of the reactor and by computational limitations. An excessively coarse mesh does not allow to catch important hydrodynamic effects such as the solid down flow along the walls. In view of the above, in this work simulations are carried out for the small scale of Tsuo (7.62 cm diameter reactor), and a scale larger by one order of magnitude (76.2 cm diameter reactor). In both cases the reactive conditions of Therdthianwong are used, that is, density of the calcined limestone of 1530 kg/m^3, sulfation reaction rate coefficient of 2.018 m^3/kmol.s, and process temperature of 1143 K. The hydrodynamic conditions, including the solid circulation rate of 24.9 kg/m^{2}s, are taken from Tsuo.

Particulate mean sizes of both authors are considered, that is, 520 μm of Tsuo and 210 μm of Therdthianwong. In both scales of reactor the same inlet velocities of gas and solid, and the same column height (5.56 m) are taken. As a consequence, the residence time of the limestone particles in the column results similar in both cases.

Table 1. Two-fluid reactive model for gas-solid flows.

Gas phase continuity

$$\frac{\partial}{\partial t}\left(\rho_g \alpha_g\right)+\vec{\nabla}\cdot\left(\rho_g \alpha_g \vec{U}_g\right)=\sum_i R_{i,g}$$

Continuity for species i in gas phase

$$\frac{\partial}{\partial t}\left(\rho_g \alpha_g Y_{i,g}\right)+\vec{\nabla}\cdot\left(\rho_g \alpha_g Y_{i,g}\vec{U}_g\right)=\vec{\nabla}\cdot\left(D_{i,g}\vec{\nabla}Y_{i,g}\right)+R_{i,g}$$

Solid phase continuity

$$\frac{\partial}{\partial t}\left(\rho_s \alpha_s\right)+\vec{\nabla}\cdot\left(\rho_s \alpha_s \vec{U}_s\right)=\sum_j R_{j,s}$$

Continuity for species j in solid phase

$$\frac{\partial}{\partial t}\left(\rho_s \alpha_s Y_{j,s}\right)+\vec{\nabla}\cdot\left(\rho_s \alpha_s Y_{j,s}\vec{U}_s\right)=\vec{\nabla}\cdot\left(D_{i,s}\vec{\nabla}Y_{j,s}\right)+R_{j,s}$$

Gas phase momentum

$$\frac{\partial}{\partial t}\left(\rho_g \alpha_g \vec{U}_g\right)+\vec{\nabla}\cdot\left(\rho_g \alpha_g \vec{U}_g \vec{U}_g\right)=-\vec{\nabla}\left(\alpha_g P_g\right)+\vec{\nabla}\cdot\left(\alpha_g \overline{\overline{\tau}}_g\right)+\rho_g \alpha_g \vec{F}_g+\beta\left(\vec{U}_s-\vec{U}_g\right)+\vec{U}_g\sum_i R_{i,g}$$

Solid phase momentum

$$\frac{\partial}{\partial t}\left(\rho_s \alpha_s \vec{U}_s\right)+\vec{\nabla}\cdot\left(\rho_s \alpha_s \vec{U}_s \vec{U}_s\right)=-\vec{\nabla}\left(\alpha_s P_s\right)+\vec{\nabla}\cdot\left(\alpha_s \overline{\overline{\tau}}_s\right)+\rho_s \alpha_s \vec{F}_s-\beta\left(\vec{U}_s-\vec{U}_g\right)+\vec{U}_s\sum_j R_{j,s}$$

Stress tensor for phase *k*

$$\overline{\overline{\tau}}_k=\mu_k\left[\vec{\nabla}\vec{U}_k+\left(\vec{\nabla}\vec{U}_k\right)^T\right]+\lambda_k\left(\vec{\nabla}\cdot\vec{U}_k\right)\overline{\overline{I}}$$

$$\mu_k = constant \qquad \lambda_k=-\tfrac{2}{3}\mu_k$$

Volumetric continuity

$$\alpha_g+\alpha_s=1$$

Solid phase pressure

$$\vec{\nabla}\left(\alpha_s P_s\right)=-G\vec{\nabla}\alpha_s+\vec{\nabla}\left(\alpha_s P_g\right)$$

$$G=exp\left[-20\left(\alpha_g-0.62\right)\right]$$

(Gidaspow and Ettehadieh, 1983)

External body forces per unit mass

$$\vec{F}_g=\vec{g} \qquad \vec{F}_s=\frac{\rho_s-\rho_g}{\rho_s}\vec{g}$$

Equations of state

$$P_g=\frac{\rho_g R_u T}{W_g} \qquad \rho_s = constant$$

Interface drag (Gidaspow, 1994)

$$\beta=150\frac{\alpha_s^2\mu_g}{\alpha_g\left(d_p\phi_s\right)^2}+1.75\frac{\rho_g\alpha_s\left|v_g-v_s\right|}{\left(d_p\phi_s\right)} \qquad for\ \alpha_s>0.2$$

(Ergun, 1952)

$$\beta=\frac{3}{4}C_{Ds}\frac{\rho_g\alpha_s\alpha_g\left|v_g-v_s\right|}{\left(d_p\phi_s\right)}\alpha_g^{-2.65} \qquad for\ \alpha_s\le 0.2$$

(Rowe, 1961)

$$C_{Ds}=\begin{cases}\dfrac{24}{Re_P}\left(1+0.15\cdot Re_p^{0.687}\right) & for \quad Re_p<1000\\ 0.44 & for \quad Re_p\ge 1000\end{cases}$$

$$Re_p=\frac{\left|v_g-v_s\right|d_p\rho_g\alpha_g}{\mu_g}$$

Reaction rate (Therdthianwong, 1994)

$$CaO+SO_2+\tfrac{1}{2}O_2\xrightarrow{K}CaSO_4$$

$$r=K\left(\frac{\rho_g\varepsilon_g Y_{SO_2,g}}{W_{SO_2}}\right)\left(\frac{\rho_s\varepsilon_s Y_{CaO,s}}{W_{CaO}}\right)$$

$$R_{SO_2,g}=-rW_{SO_2} \qquad R_{CaO,s}=-rW_{CaO}$$

$$R_{O_2,g}=-\tfrac{1}{2}rW_{O_2} \qquad R_{CaSO_4,s}=rW_{CaSO_4}$$

Symbols

C_D	drag coefficient, non-dimensional	W	molecular weight, kg/kmol
d_p	particle diameter, m	u,v,w	velocity components, m/s
D	mass diffusion coefficient, kg/m s	Y	mass fraction, $kg_{i,j}/kg_k$
$\overline{\overline{D}}$	viscous stress tensor rate, 1/s	Greek	
$\vec{F}$	external body force per unit mass, m/s^2	α	volume fraction, m_k^3/m^3
$\vec{g}$	gravity acceleration, m/s^2	β	gas-solid friction coefficient, $kg/m^3 s$
G	particle-particle elasticity modulus, N/m^2	λ	bulk viscosity, $N\ s/m^2$
K	reaction rate coefficient, $m^3/kmol\ s$	μ	dynamic viscosity, $N\ s/m^2$
P	pressure, N/m^2	ρ	density, kg/m^3
r	molar reaction rate, $kmol/m^3 s$	$\overline{\overline{\tau}}$	viscous stress tensor, N/m^2
R	mass reaction rate, $kg/m^3 s$	φ	particle sphericity, non-dimensional
R_u	ideal gas constant, kJ/kmol K	Subscripts	
Re_p	Reynolds number, non-dimensional	g	gas phase
t	time, s	i,j	chemical species
T	temperature, K	k	either gas or solid phases
$\vec{U}$	average velocity vector, m/s	s	solid phase

Four different operational conditions were simulated considering the combination of the two different reactor diameters and the two particulate sizes. An additional case was simulated extending to 15 m the height of the reactor in one of the previous operational conditions. This allowed to observe the effect of a higher residence time on SO_2 absorption.

Steady state convergence was achieved in only one of the considered cases (reactor 7.62 cm, particulate 210 μm). For this case the hydrodynamic results showed no presence of any coherent structures. In the cases where steady state solutions were not found, the impossibility of convergence is attributed to flow inherent instabilities associated to the development of coherent gas-solid structures. A discussion on this matter is presented in Milioli and Milioli (2005). Despite not converged, the iterative procedure provided results showing the expected presence of coherent structures. While quantitatively meaningless since no convergence was reached, those results allowed some qualitative analysis regarding the effect of the coherent structures on sulfur absorption.

All the simulations were performed for the same 3D cylindrical geometry shown in Tab. 2. The table also describes all the cases considered, and shows properties, initial and boundary conditions, details of the numerical tetrahedral meshes that were used, and numerical settings. Three-dimensional isothermal steady state simulations were performed. Air was taken as the fluidizing gas at pressure, temperature, flow rate and SO_2 fraction typical of coal combustion. The solid phase was assumed to be comprised of limestone both calcined and sulfated, and inert silica simulating the physical presence of coal and ashes.

Table 2. Geometry and settings.

Column

Mesh 1

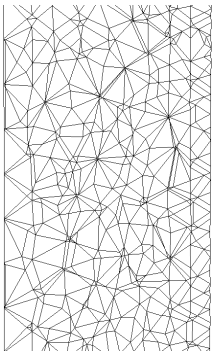

height section

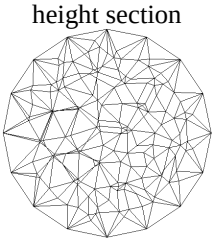

cross section

Cases	Mesh	Particle size (μm)	Column diameter (cm)	Column height (m)
A	1	210	7.62	5.56
B	1	520	7.62	5.56
C	2	210	7.62	15.0
D	3	210	76.2	5.56
E	3	520	76.2	5.56

Numerical conditions			
Meshes	1	2	3
Tetrahedrals	206229	556588	206236
Nodes (total)	42029	113508	39538
Nodes (cross section / 3.4 m)	226	268	1044
Convergence: $rms = 1 \times 10^{-5}$ for all variables			

Phases	Species
$g =$ gas at 870 °C	$i = N_2, O_2, SO_2$
$s =$ solid at 870 °C	$j = CaO, CaSO_4, SiO_2$
Properties	
$\rho_{N_2} = 0.2952$ kg/m^3	$\rho_{SiO_2} = 2650$ kg/m^3
$\mu_{N_2} = 4.294 \times 10^{-5}$ N/m^{2}s	$\mu_{SiO_2} = 0.509$ N/m^{2}s
$W_{N_2} = 28$ kg/kmol	$W_{SiO_2} = 60$ kg/kmol
$\rho_{O_2} = 0.3372$ kg/m^3	$\rho_{CaO} = 1530$ kg/m^3
$\mu_{O_2} = 5.133 \times 10^{-5}$ N/m^{2}s	$\mu_{CaO} = 0.509$ N/m^{2}s
$W_{N_2} = 32$ kg/kmol	$W_{CaO} = 56$ kg/kmol
$\rho_{SO_2} = 0.6828$ kg/m^3	$\rho_{CaSO_4} = 2875$ kg/m^3
$\mu_{SO_2} = 4.23 \times 10^{-5}$ N/m^{2}s	$\mu_{CaSO_4} = 0.509$ N/m^{2}s
$W_{SO_2} = 64$ kg/kmol	$W_{CaSO_4} = 136$ kg/kmol
$D_{O_2} = 0.67 \times 10^{-4}$ kg/m s	$D_{CaO} = 0$ kg/m s
$D_{SO_2} = 1.36 \times 10^{-4}$ kg/m s	$D_{CaSO_4} = 0$ kg/m s
Boundary conditions	
Inlet	
$u_g = 0$ m/s	$u_s = 0$ m/s
$v_g = 4.979$ m/s	$v_s = 0.408$ m/s
$w_g = 0$ m/s	$w_s = 0$ m/s
$\alpha_g = 0.9754$ m$_g^3$/m^3	$\alpha_s = 0.0246$ m$_s^3$/m^3
$Y_{O_2,g} = 0.23243$ kg$_{O_2}$/kg$_g$	$Y_{CaO,s} = 0.15$ kg$_{CaO}$/kg$_s$
$Y_{SO_2,g} = 0.00443$ kg$_{SO_2}$/kg$_g$	$Y_{CaSO_4,s} = 0$ kg$_{CaSO_4}$/kg$_s$
Outlet	Walls
Locally parabolic	$g =$ non-slipping
$P_g = 64$ N/m^2 (relative)	$s =$ free slip
Initial conditions - as in the inlet, except:	
$\alpha_g = 0.62$ m$_g^3$/m^3	$\alpha_s = 0.38$ m$_s^3$/m^3
Chemical reaction (Therdthianwong, 1994)	
$CaO + SO_2 + \frac{1}{2}O_2 \xrightarrow{K} CaSO_4$	
$K = 2.018$ m^3/kmol s	

4. Results and discussion

Steady state convergence of the numerical procedure was achieved only for case A (as defined in Tab. 2). The convergence was reached after 3862 iterations of the numerical procedure. In all the other cases there was no convergence (cases B, C, D and E as defined in Tab. 2). However, the outputs after 10000 iterations of the numerical procedure are presented for all the not converged cases. Despite not converged, the results show a correct hydrodynamics and allow a qualitative analysis of the effects of coherent structures on sulfur absorption.

Figures 1 to 8 show results in the column cross section 3.4 m above entrance. Those are radial profiles of vertical gas and solid velocities, solid volume fraction, and SO_2 mass fraction. Figures 1 and 2 present results for the converged case A. It is seen that he solid volume fraction results uniform in the cross section of the column, the solid results uniformly distributed, and no clusters are developed in the flow field. Velocity profiles result symmetrical owing to flow homogeneity, and flat showing that the uniform drag overcomes viscous effects. SO_2 mass fraction also results uniform as a consequence of solid distribution uniformity. As discussed in Milioli and Milioli (2005), the above uniformities are unreal, and should be attributed to numerical diffusion.

Figures 3 to 8 present results for the non converged cases B, D and E. Non uniform asymmetrical profiles are observed for all the variables, which is typical of flows where clusters are developed. Negative velocities are found close to the walls showing the expected solid down flow regime typical of risers as well as the down flow of clusters. For the larger section reactor case D the solid volume fraction results higher at the walls and flat through the core, characterizing a core annular flow. For the smaller section reactor case B the wall effect combined with the development of clusters prevents the core annulus to be developed. SO_2 mass fraction results non uniform as a consequence of solid distribution non uniformity. As expected, SO_2 mass fraction results lower where solid fraction is higher. All the above results are qualitatively coherent with empirical observation, even for the non converged cases.

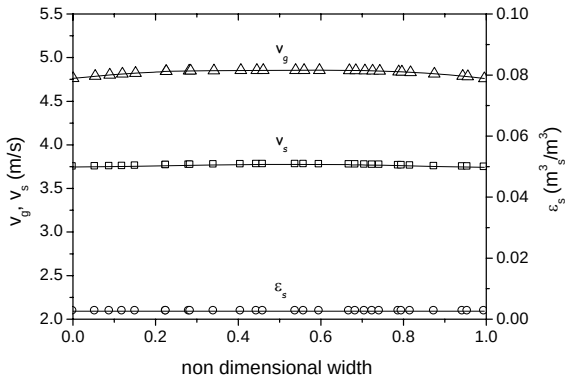

Figure 1. v_g , v_s and ε_s 3.4 m above entrance - Case A.

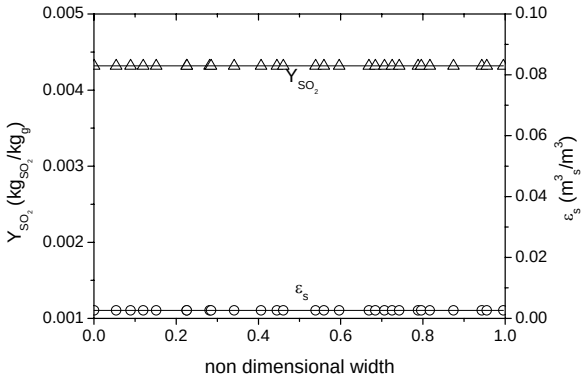

Figure 2. $Y_{SO_2,g}$ 3.4 m above entrance - Case A.

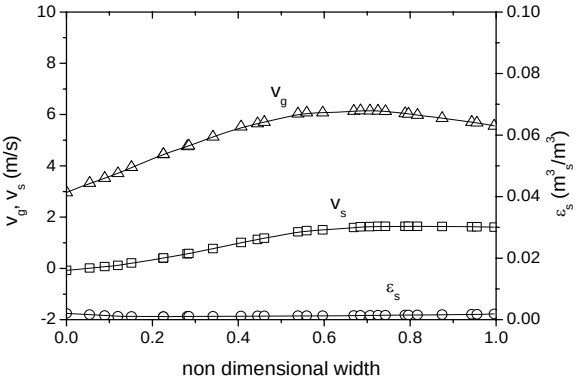

Figure 3. v_g , v_s and ε_s 3.4 m above entrance - Case B.

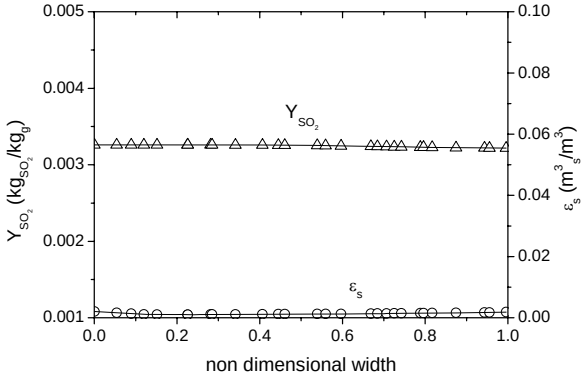

Figure 4. $Y_{SO_2,g}$ 3.4 m above entrance - Case B.

Figures 9 to 12 show axial profiles of cross section area averaged solid volume fractions, solid velocities, solid circulation rates, and SO_2 mass fractions for all the cases. The converged case A presents well behaved profiles owing to the homogeneity of the flow. The non converged cases show scattered irregular profiles owing to the effect of clusters. Figure 9 shows that in all the cases the solid volume fractions are mostly inside the expected from experiment (below 3% according to Sun, 1996). As seen in Fig. 10, lower solid velocities are found for the larger 520 μm particulate, as expected (cases D and E). Figure 11 shows that, except for the converged case A, the solid circulation

rate results very far away from the expected 24.9 kg/m^{2}s. This means that mass conservation is not reached for the non converged cases. Therefore, while allowing some qualitative analysis, the non converged results present no quantitative accuracy.

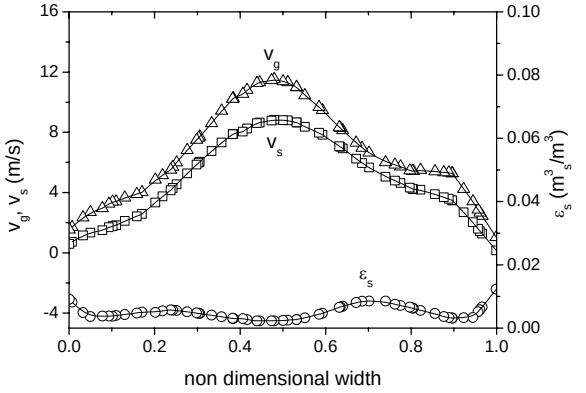

Figure 5. v_g , v_s and ε_s 3.4 m above entrance - Case D.

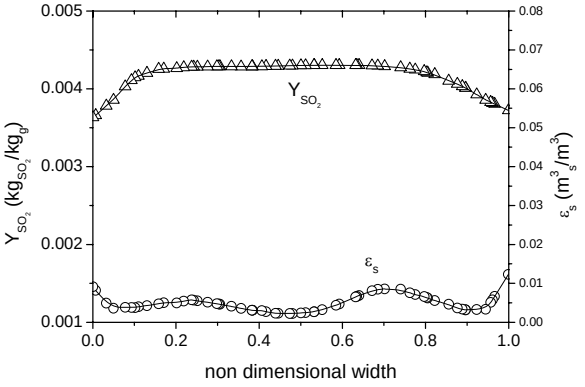

Figure 6. $Y_{SO_2,g}$ 3.4 m above entrance - Case D.

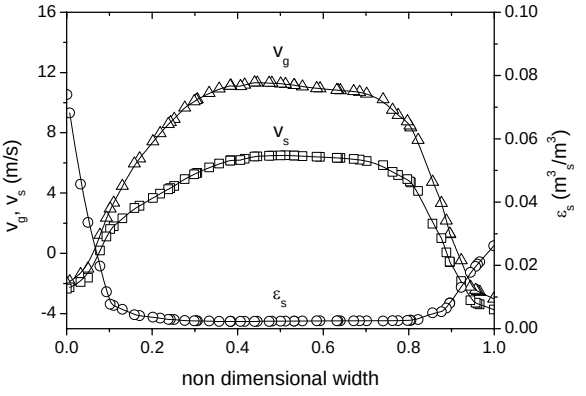

Figure 7. v_g , v_s and ε_s 3.4 m above entrance - Case E.

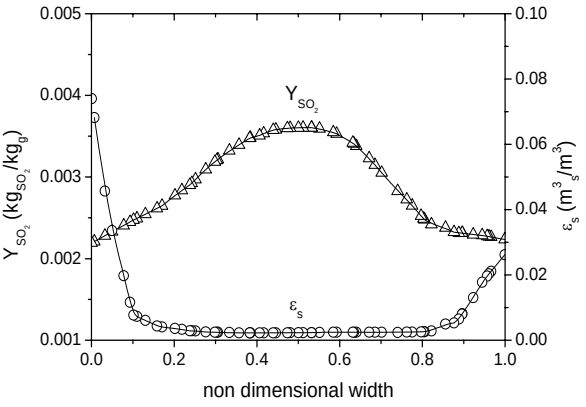

Figure 8. $Y_{SO_2,g}$ 3.4 m above entrance - Case E.

Figure 12 shows that the larger the particles the higher the reduction on SO_2 mass fraction along column's height. The results for cases B and E (larger particles) compared to those for cases A, C and D (smaller particles) show this fact. Such behavior is in fact expected since the only effect of particle size accounted for by the model concerns drag. Larger particles present higher terminal velocities and, therefore, higher residence times, providing higher sulfur removal. As far as particle size is concerned, in real absorption columns sulfur removal depends on the balance of opposing effects of residence time and reaction rate. Larger particles provide higher residence times, which contributes for higher absorption. On the other hand, larger particles provide lower reaction rates, which contributes for lower absorption. The concerning balance can not be evaluated through the present simulations since the model does not include dependence of reaction rate with particle size.

Figure 12 also shows that the wider the column the higher the reduction of SO_2 mass fraction. For instance, the results for case B (narrower column) compared to those of case E (wider column) show this fact. Such behavior does not seem correct since in the narrower column residence time results higher owing to lower solid axial velocities (as seen in Fig. 10). It should be remembered here that the present results lack accuracy since there is no convergence of the numerical procedure. Such trend may account for the wrong predictions. Anyway, the discrepancy concerning column width must be further investigated.

Another feature observed in Fig. 12 concerns the effect of column height on sulfur absorption. A comparison of results for the higher column of case C with those for the shorter column A, at the same height, shows the higher column provides higher absorption. This is a clear consequence of the higher residence time provided by clusters, which are caught in the higher column and are not in the shorter one. As far as clusters are concerned, in real absorption columns sulfur removal depends on the balance of opposing effects of residence time and gas-solid contact. Clusters provide higher residence times, which contribute for higher absorption. On the other hand, clusters impose higher resistances to mass transport, which contribute for lower absorption. The above balance can not be evaluated from the present simulations since the model does not include dependence of reaction rate with solid phase fraction.

Figure 13 shows grayscale plots of the solid volume fraction through a central vertical plan along the column's height, for all the cases. In opposition to case A, where a homogeneous flow is seen, in all the other cases clusters are clearly observed.

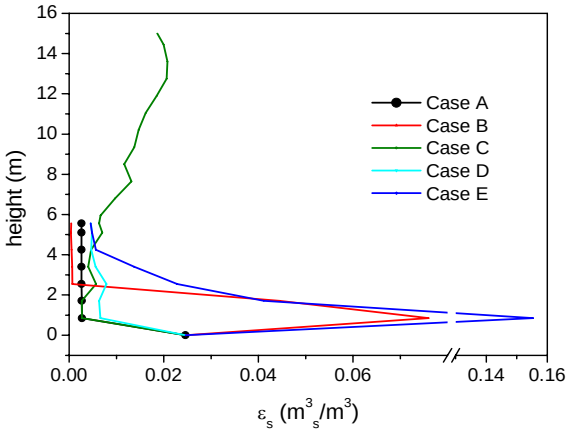

Figure 9. Axial profiles of area averaged ε_s.

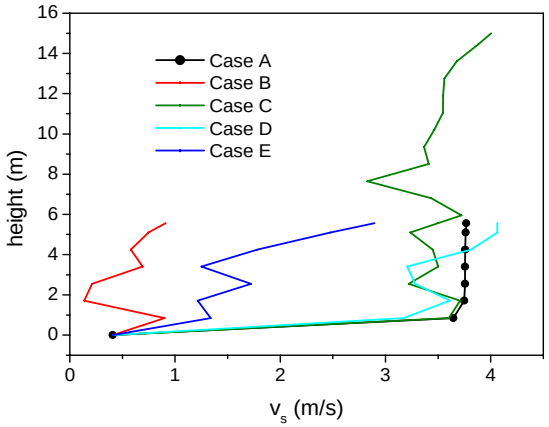

Figure 10. Axial profiles of area averaged v_s.

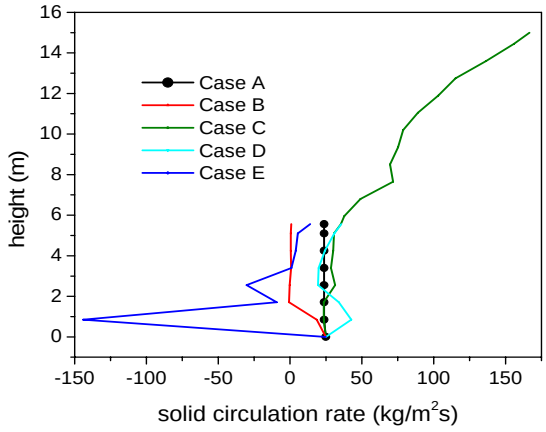

Figure 11. Axial profiles of solid circulation rate.

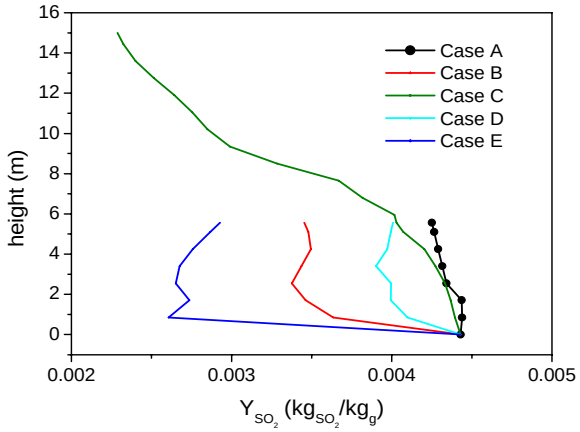

Figure 12. Axial profiles of area averaged $Y_{SO_2,g}$.

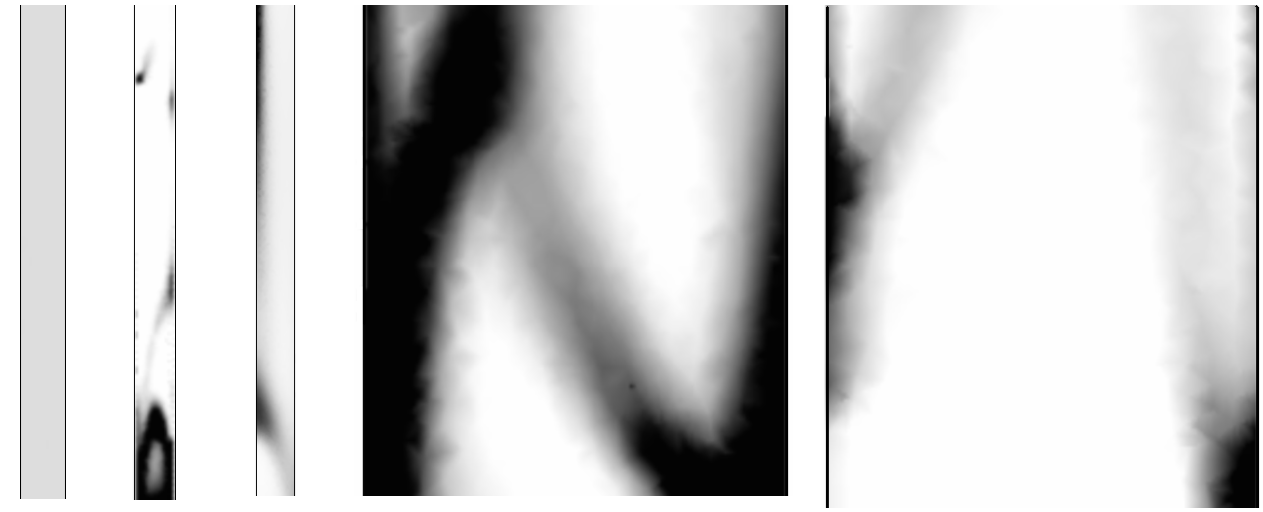

Figure 13. Grayscale plots of ε_s through a central vertical plan along the column's height.

5. Conclusions

Five different setups of circulating fluidized bed riser flows were simulated. Convergence was reached in only one of the cases, for which the flow resulted homogeneous and free of coherent structures. SO_2 mass fraction resulted uniform as a consequence of solid distribution uniformity. Those uniformities are anomalous and should be credited to numerical diffusion. In all the other cases considered, there was no convergence, which was credited to physical instabilities inherent to the gas-solid flows as coherent structures are continuously formed and dissipated. In those cases SO_2 mass fraction resulted non uniform as a consequence of solid distribution non uniformity. Mass conservation was not reached for the non converged cases. Therefore, while allowing some qualitative analysis, the non converged results present no quantitative accuracy.

The present simulations indicate that coherent structures benefit chemical reaction by increasing residence times. Otherwise, coherent structures also difficult gas-solid contact and should difficult chemical reaction. This late feature is not accounted for in the present two-fluid reactive models. In the present simulations a constant chemical reaction rate coefficient was assumed irrespective of particulate size and flow hydrodynamics. Unfortunately, SO_2 absorption is very dependent on both. It seems that better empirical data are required so that better analyses can be done from predictions. It is quite clear that the models need to be improved. Properties such as solid phase viscosity and pressure, and drag coefficients, need to be accurately correlated to parameters such as solid fraction. Reaction rate coefficients must be accurately correlated to particle size, and must incorporate the resistance to reaction due to mass transfer in the fluidized ambience. Unfortunately, the current state of the art in circulating fluidized bed reactive processes does not provide the above information, whether theoretically or empirically. Besides model improvements, simulations are required to be transient so that accurate quantitatively meaningful predictions can be made.

6. Acknowledgements

This work was supported by FAPESP and CNPq.

7. References

CFX 5.7, 2004a, " Multiphase Flow Theory", in Solver Theory Manual, Ed. Ansys Canada Ltda, pp. 105-160.

CFX 5.7, 2004b, " Multiphase Flow Modelling", in Solver Modelling Manual, Ed. Ansys Canada Ltda, pp. 147-206.

CFX 5.7, 2004c, "Discretization and Solution Theory", in Solver Theory Manual, Ed. Ansys Canada Ltda, pp. 147-206.

Enwald, H., Peirano, E. and Almstedt, A.-E., 1996, "Eulerian Two-Phase Flow Theory Applied to Fluidization", Int. J. of Multiphase Flow, Vol. 22, pp.21-66.

Ergun, S., 1952, "Fluid Flow through Packed Columns", Chem. Engng. Prog., Vol. 48, No. 2, pp 89-94.

Gidaspow, D. and Ettehadieh, B., 1983, "Fluidization in two-dimensional debs with a jet. Part II. Hydrodynamic modeling", Indust. Engng. Chem. Fundam., Vol. 22, pp. 193-201.

Gidaspow, D., 1994, "Multiphase Flow and Fluidization", Academic Press, San Diego, CA, 407p.

Grace, J.R. and Bi, H., 1997, "Introducyion to Circulating Fluidized Beds", in Circulating Fluidized Beds, Ed. J.R. Grace, A.A. Avidan and T.M. Knowlton, Chapman & Hall, UK, 585p.

Jenkins, J.T. and Savage, S.B., 1983, "A Theory for the Rapid Flow of Identical, Smooth, Nearly Elastic Spherical Particles", J. Fluid. Mech., Vol. 130, pp. 187-202.

Lun, C.K.K., Savage, S.B., Jeffrey, D.J. and Chepurniy, N., 1984, "Kinetic Theories for Granular Flows: Inelastic Particles in Couette Flow and Singly Inelastic Particles in a General Flow Field", J. Fluid. Mech., Vol. 140, pp.223-256.

Milioli, C.C.C. and Milioli, F.E., 2005, "Steady State Simulation of Hydrodynamics in Circulating Fluidized Beds", Proceedings of the 18th International Congress of Mechanical Engineering, Ouro Preto, Brazil.

Rowe, P.N., 1961, "Drag Forces in a Hydraulic Model of a Fluidized Bed. Part II", Trans. IChemE, Vol. 39, pp. 175-180.

Sun, B., 1996, "Simulation of gas-liquid and gas-solid two phase flows", PhD thesis, Illinois Institute of Technology, Chicago, Illinois, 231p.

Therdthianwong, A., 1994, "Hydrodynamics and SO_2 Sorption in a Circulating Fluidized Bed", PhD thesis, Illinois Institute of Technology, Chicago, Illinois, 219p.

Tsuo, Y.P., 1989, "Computation of Flow Regimes in Circulating Fluidized Beds", PhD thesis, Illinois Institute of Technology, Chicago, Illinois, 208p.

8. Responsibility notice

The authors are the only responsible for the printed material included in this paper.